AIAA 81-0683R

Thrust Measurement of KIII MPD Arcjet

K. Kuriki* and M. Onishi†
Institute of Space and Astronautical Science, Tokyo, Japan
and
S. Morimoto‡
Ishikawajima-Harima Heavy Industries Co., Ltd., Yokohama, Japan

A quasisteady MPD arcjet, KOMABA III, has been studied to obtain its fundamental characteristics as a thruster. KIII was provided with new devices, such as auxiliary electrodes at floating potential and gas injection from various gas ports in the discharge chamber. Propellant injection near the anode surface resulted in a decrease of anode fall voltage and enhancement of thrust efficiency. Injection near the cathode base increased the collisionless nature of the acceleration mechanism and diminished efficiency. A sleeve electrode mounted coaxially to the cathode around the root was found to buffer the concentration of discharge current.

Introduction

IT has been noted in the research on MPD arcjets that the upper limit of the discharge current exists for the operation free of significant electrode erosion with propellant flow rate fixed. The studies have focused on enlarging the current range in which the arcjet can be operated without erosion. Several methods have been proposed: 1) The effect of propellant distribution has been studied in various configurations: injections from base plate, cathode root,[1] and anode exit[2,3]; 2) selection of electrode geometry; e.g., varying the distribution of discharge current by geometry modification[4]; 3) use of heat-resistive material for electrodes and insulator; and 4) application of an external magnetic field, although field application imposes a penalty of extra power and degrades the simplicity of the self-field accelerator.

In the present experiment a new, quasisteady MPD arcjet, KOMABA III (KIII), was used. The discharge chamber of the new model was provided with three gas ports and with auxiliary electrodes at floating potential. With these devices, the present study intends to answer the following questions:

1) How are the thrust and discharge voltage, and the resulting efficiency, influenced by propellant distribution?

2) How are the anode and cathode falls affected by the method of propellant injection?

3) How is the concentration of discharge current at the cathode root relaxed by gas injection and the auxiliary electrode near the cathode? It was found in companion studies that the large current concentrates at the cathode base.[4]

Except for the provisions mentioned previously and the slightly enlarged dimensions of the electrode system, the discharge chamber of the new model had almost the same configuration as that used in the authors' previous studies.[3,5] The results obtained in the present experiment, therefore, can be discussed in reference to those in previous studies.

Experimental Apparatus

The cross-sectional view of the KIII discharge chamber is shown in Fig. 1. In the discharge chamber are three annular slits from which the propellant is injected. Anode injection from inside (AII) is gas injection between the anode inner surface and the floating electrode (AFI) covering the outside surface of the base insulator. Anode injection from outside (AIO) is injection between the anode outer surface and the inner surface of the outermost floating electrode (AFO). Cathode injection (CI) is injection between the cathode outer surface and the inner surface of the floating electrode (CF) with which the inside surface of the base insulator was lined. The mass flow rate $\dot{m}$ of Ar propellant at these ports was controlled by a fast-acting valve (FAV) and ranged from 0.05 to 1.3 g/s.

The role of the floating electrodes was threefold. First, they monitored the azimuthally averaged floating potential. Second, the floating electrodes were useful in relaxing current concentration near the base-plate boundaries neighboring the anode and the cathode. Especially together with the CF electrode, the cathode root forms an annular hollow cathode. A part of the discharge current can creep into the narrow annular region and gradually drain into the cathode. The CF electrode and the cathode were heat-sunk and kept the plasma away from the annular region. The same effects were expected from the AFI and AFO electrodes. Third, the floating electrodes prevented the insulator from directly touching the discharge plasma carrying the current. The material was

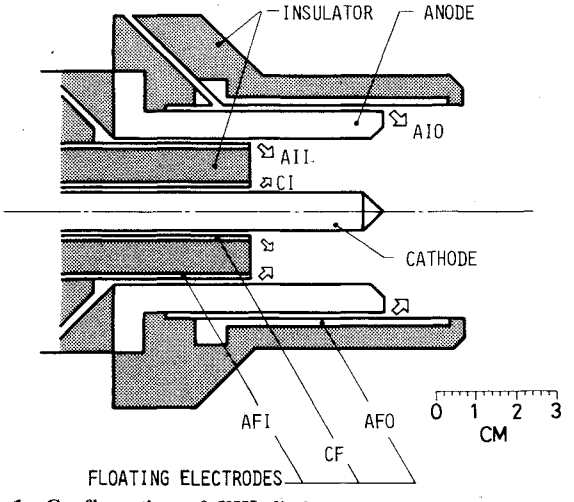

Fig. 1 Configuration of KIII discharge chamber: AII, anode injection from inside; AIO, anode injection from outside; CI, cathode injection.

Presented as Paper 81-0683 at the AIAA/JSASS/DGLR 15th International Electric Propulsion Conference, Las Vegas, Nev., April 21-23, 1981; submitted April 29, 1981; revision received Feb. 25, 1982.

*Professor. Member AIAA.
†Graduate Student; presently at Toshiba Corp., Kawasaki, Japan.
‡Chief Research Engineer. Member AIAA.

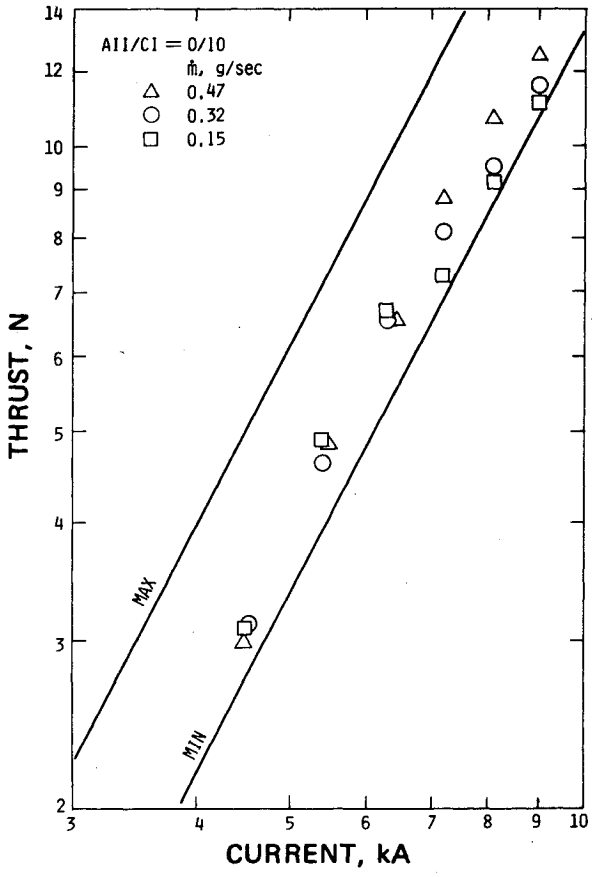

Fig. 2 Thrust-current characteristics for AII/CI = 0/10. Solid lines represent theoretical predictions. MAX: $T_{max} = 10^{-7}$ $[\ell n(r_a/r_c) + 3/4]J^2$ with $r_a/r_c = 49/9.5$; MIN: $T_{min} = 10^{-7}$ $[\ell n(r_a/r_c)]J^2$ with $r_a/r_c = 36/9.5$.

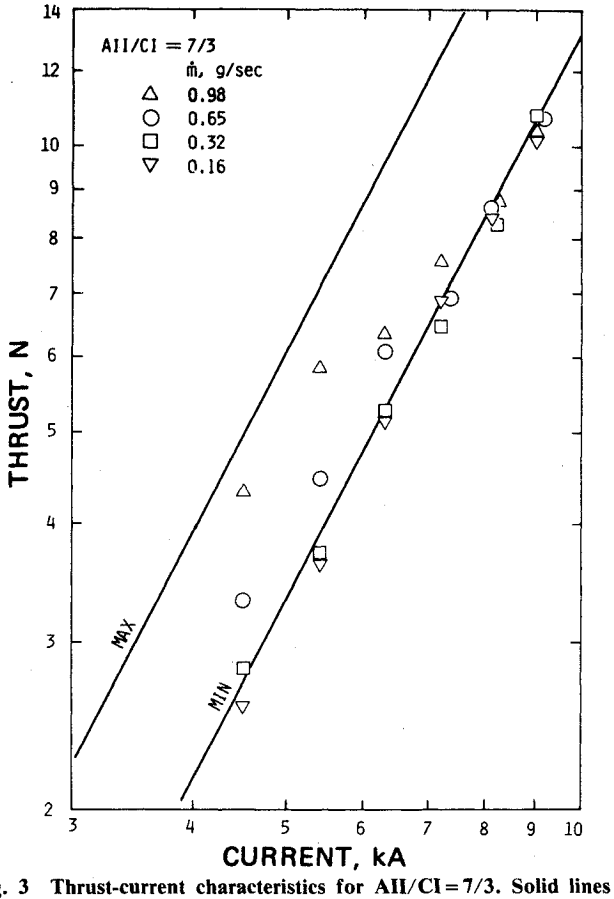

Fig. 3 Thrust-current characteristics for AII/CI = 7/3. Solid lines represent theoretical predictions. MAX and MIN are the same as in Fig. 2.

copper for AFI and AFO and tantalum for CF. Another cathode rod was fabricated so as to have two current-collecting areas separated by an insulator: one surface was exposed to the discharge chamber and the other to the annular hollow region. With this cathode, the cathode current in the annular region was measured separately.

The power-supplying pulse-forming network (PFN) and the vacuum tank in which the arcjet was fired were the same as those used in previous studies.[3,5] The maximum discharge current was 10 kA and the pulse width was 1 ms. Tank pressure before discharge was 10^{-5} Torr. The discharge chamber was mounted together with FAV on a bed suspended by wires that terminated at the tank ceiling. Displacement of the bed was detected by a linear differential transformer. Impulse-displacement calibration was made by applying known impacts. The image of the plasma at 3 cm downstream of the arcjet exit was focused on the slit of a spectrometer to monitor argon, tungsten, and copper spectral lines. The image size being less than the slit height, light emission was collected from the entire cross section of the plasma stream.

Experimental Results

The measured thrust T is plotted against discharge current in Figs. 2, 3, and 4 for AII/CI = 0/10, 7/3, and 10/0, respectively. Here, AII/CI = 7/3 means that 70% of the total mass flow rate is allotted for AII and 30% for CI. The solid lines labeled "MIN" and "MAX" represent theoretical predictions as follows:

$$\text{MAX: } T = (\mu/4\pi)J^2[\ell n(r_a/r_c) + 3/4] \quad (1)$$

$$\text{MIN: } T = (\mu/4\pi)J^2\ell n(r_a/r_c) \quad (2)$$

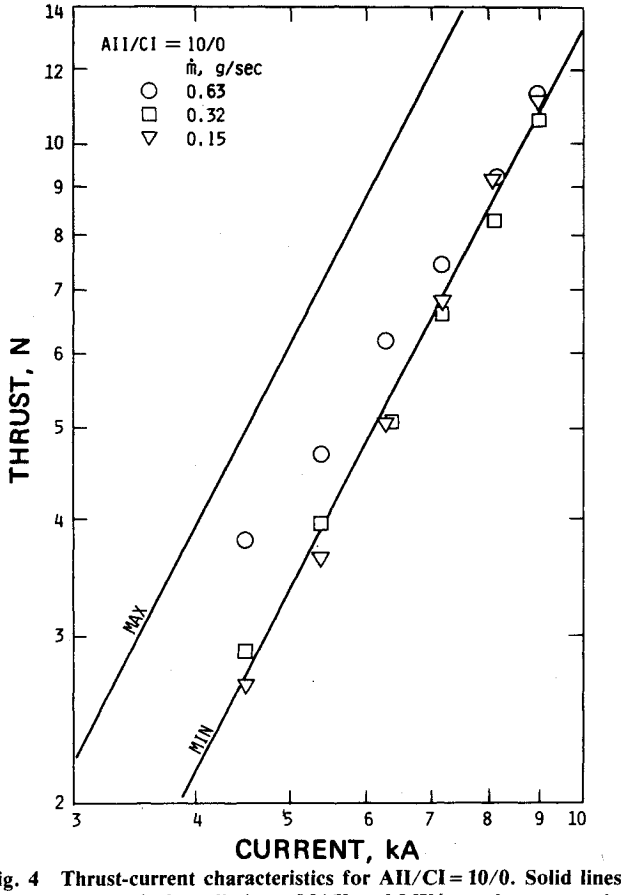

Fig. 4 Thrust-current characteristics for AII/CI = 10/0. Solid lines represent theoretical predictions. MAX and MIN are the same as in Fig. 2.

where μ is permeability and r_a and r_c are the anode and cathode radii, respectively. In Fig. 2 are shown the thrust-current characteristics for AII/CI = 0/10. The thrust is greater than the MIN value and close to the relation

$$T = (\mu/4\pi) J^2 [\ell n (r_a/r_c) + 1/4] \quad (3)$$

Aerodynamic thrust, which would be linearly proportional to J, is not observed even at large mass flow rate. This result is rather contrary to the authors' expectation that the propellant distribution near the cathode might effectively exert pressure on the cathode tip and the base plate. When the mass flow near the anode surface was added, the thrust at high current decreased significantly, as shown in Fig. 3 for the case of AII/CI = 7/3, i.e., slightly below the MIN prediction. The result for AII/CI = 7/3 is similar to that in the authors' previous experiment.[5] At largest $\dot{m}$ and low current, however, the thrust exceeded the MIN value and showed the characteristics of aerodynamic acceleration, i.e., the relation $T \propto J$. As shown in Fig. 4, when the propellant supply from the cathode root was shut off totally, the aerodynamic effect was found to be slightly enhanced or saturated when the data at $\dot{m} = 0.63$ g/s for AII/CI = 10/0 and those at $\dot{m} = 0.65$ g/s for AII/CI = 7/3 were compared.

The results of voltage measurement are shown in Figs. 5 and 6. The discharge voltage and the anode and cathode fall voltages that were measured by the floating electrodes AFI and CF are plotted in Fig. 5 for AII/CI = 0/10. Comparing with the former results,[3,5] the discharge voltage in the AII/CI = 0/10 case was very high at large $\dot{m}$ and small J. It was distinctly observed in Fig. 5, especially at small $\dot{m}$, that the discharge voltage stalled after exhibiting a maximum. Similar features were found in the results of anode fall voltage in a much more distinct manner. Furthermore, the anode fall voltage was as high as 100 V, in contrast to the handbook knowledge of about 5 V for the atmospheric arc. The cathode fall voltage, on the other hand, stayed low and close to the values of the atmospheric arc. When the anode fall voltage was measured near the anode exit by the AFO electrode, the result was much lower than the AFI voltage. This implies that the anode fall voltage depends strongly on streamwise location. It may be possible that an anode fall voltage higher than those shown in Fig. 5 will appear between the base plate and the anode exit. The discharge voltage decreases significantly when the mass flow from the anode root is turned on, as shown in Fig. 6. The anode fall voltage in the AII/CI = 7/3 case lies below 20 V at large $\dot{m}$ and small J,

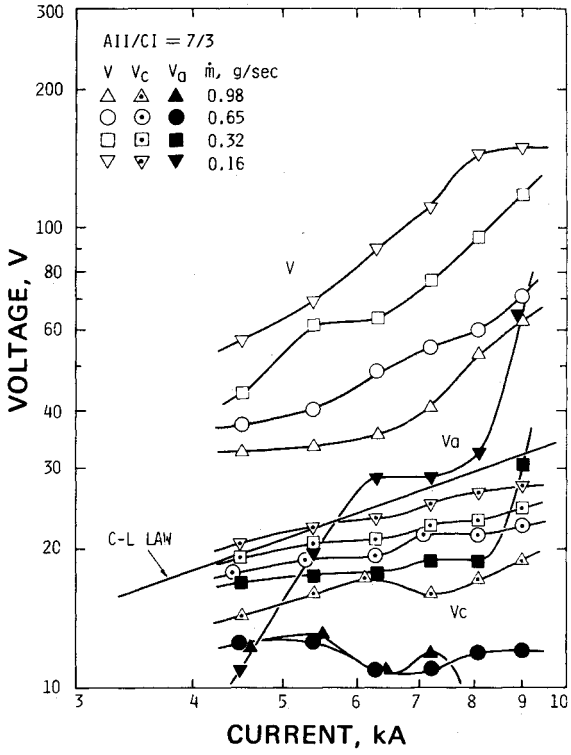

Fig. 6 Voltage-current characteristics for AII/CI = 7/3. V, V_a, and V_c are the same as in Fig. 5. C-L (Child-Langmuir) law: $j = (4\epsilon_0/9)(2e/m_i)\lambda_D^{-2} V_0^{2/3}$, $T_e = 3$ eV, $N_e = 10^{15}$ cm^{-3}, $j = 10^7$ A/m^2.

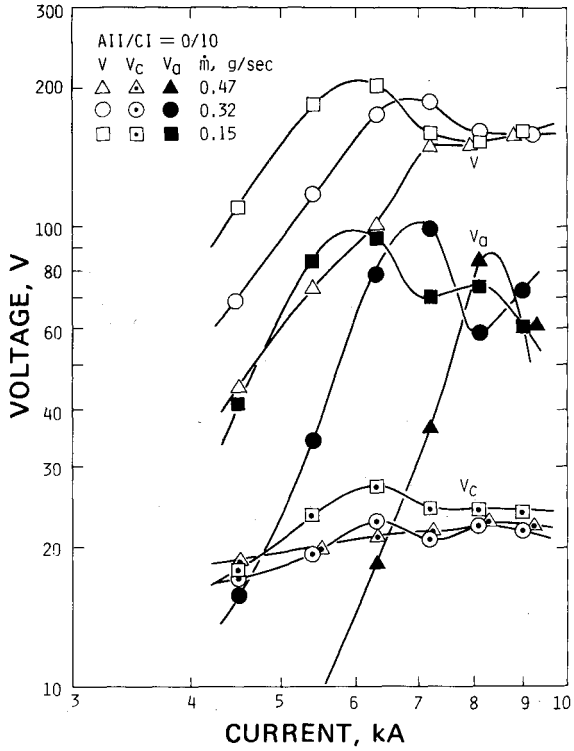

Fig. 5 Voltage-current characteristics for AII/CI = 0/10: V, discharge voltage; V_a, anode fall voltage; V_c, cathode fall voltage.

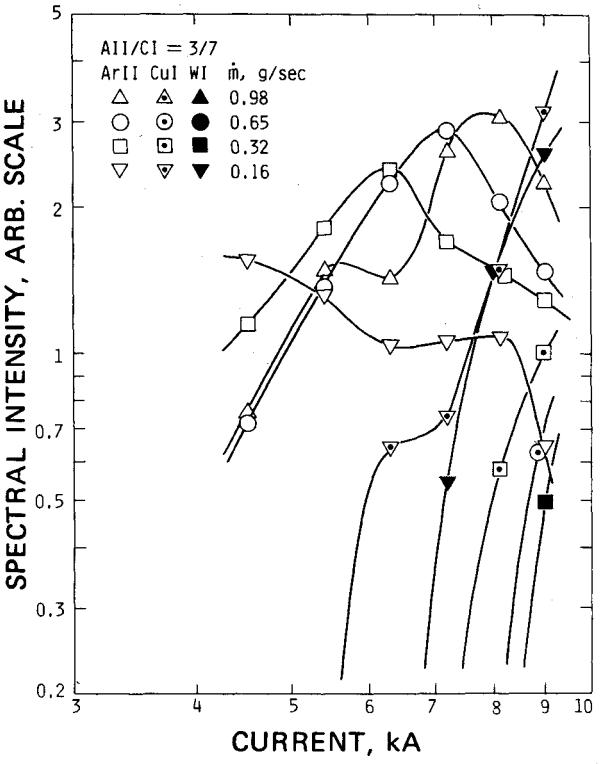

Fig. 7 Spectral intensity of ArII, CuI, and WI lines for AII/CI = 3/7.

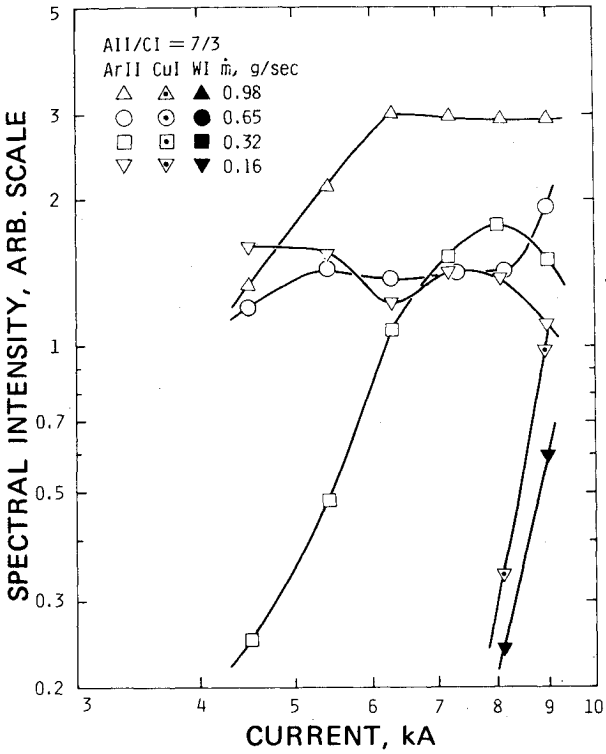

Fig. 8 Spectral intensity of ArII, CuI, and WI lines for AII/CI = 7/3.

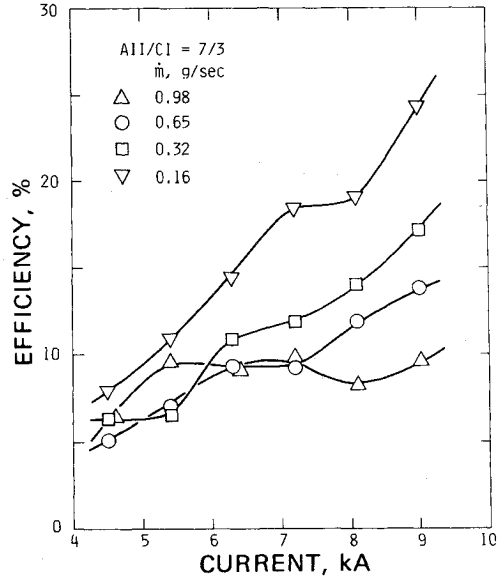

Fig. 9 Efficiency for AII/CI = 7/3.

whereas it increases sharply at small $\dot{m}$ and large J. The cathode fall voltage is less than 30 V and follows approximately the $J^{2/3}$-dependence predicted by the Child-Langmuir law.

Qualitative observation of argon ion, tungsten atom, and copper atom lines was made to assess the upper limit of thruster performance obtained by the thrust and voltage measurements. A simple criterion was adopted to determine the limit: the spectral intensity of ArII (5009 Å) should be less than or equal to those of WI (5006 Å) and CuI (4076 Å). This criterion is crude since transition probability and detector sensitivity are different among the spectral lines. If one looks at the rapid increase in the spectral intensity of impurities in Figs. 7 and 8, however, the detailed structure of emission can be ignored in an approximate account. In the AII/CI = 0/10 case, the impurity emission exceeded ArII emission in most of the operating conditions. Therefore, the graphical presentation is given for AII/CI = 3/7 and 7/3 in Figs. 7 and 8, respectively. In both figures the intensity of ArII emission saturates or tends to decrease at high discharge current and is exceeded by the intensity of impurity emission. Comparing the results in Figs. 7 and 8, the impurity emission starts at lower discharge current for a smaller mass flow rate of AII. Thrust efficiency calculated from thrust and input power is plotted in Fig. 9 for AII/CI = 7/3. All the points in Fig. 9 satisfy the criterion on impurity emission.

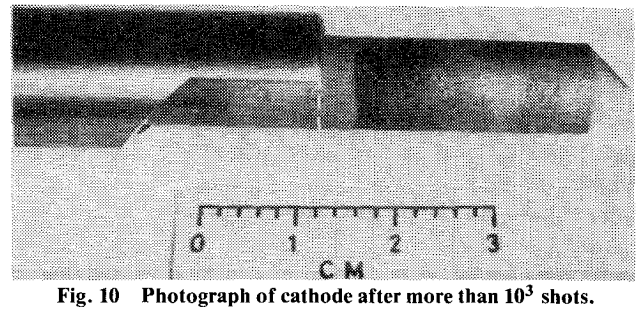

Fig. 10 Photograph of cathode after more than 10^3 shots.

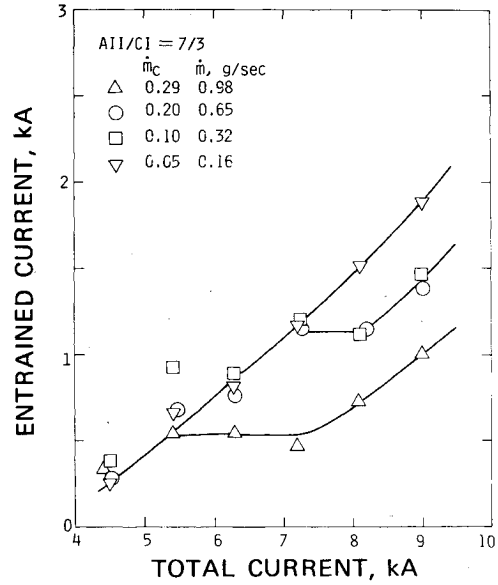

Fig. 11 Discharge current entrained in annular region for AII/CI = 7/3. $\dot{m}_c$ is the flow rate of the propellant injected in the annular region.

The electrode CF at floating potential was coaxially assembled with the rod cathode. The spacing between CF and cathode was 1 mm. As demonstrated in Fig. 10, the cathode surface at the CF edge or base-plate surface was smoothly burned by the arc discharge and had no crater on the surface. The photograph was taken after more than 1000 shots. The burned surface condition was gradually faded toward upstream and turned into a machined surface. The burned region was about 10 times as large as the electrode gap. The discharge current in the annular region was measured by the cathode with divided surfaces, and is plotted against the discharge current in Fig. 11. The current entrained in the annular region was as large as 20% of the total current. At large discharge current, the fraction of entrained current was larger for the smaller propellant flow rate. These results support the buffering effect of the CF electrode on discharge current concentration.

Discussion

Anode fall plays a key role in determining MPD arcjet performance. If the measured voltages are replotted in a

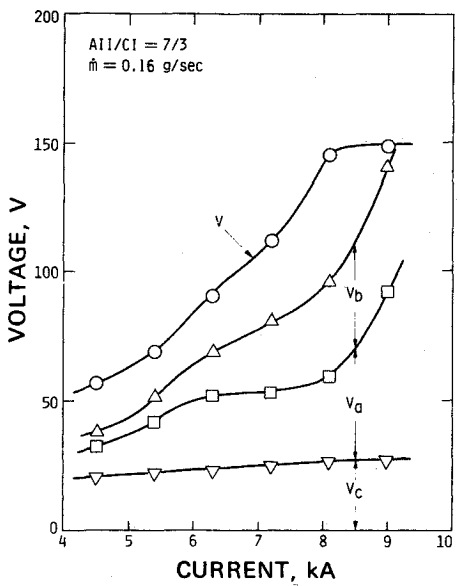

Fig. 12 Voltage-current characteristics for AII/CI = 7/3. $\dot{m} = 0.16$ g/s. V, discharge voltage; V_a, anode fall voltage; V_b, acceleration voltage; V_c, cathode fall voltage.

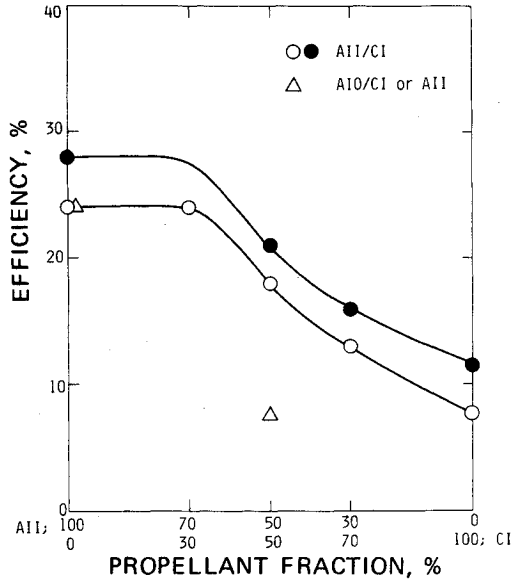

Fig. 13 Maximum efficiency vs propellant fraction. Open symbols are compatible with the spectral emission criterion; solid symbols are incompatible.

cumulative manner, as shown in Fig. 12, the anode fall voltage is found to be 30% of the discharge voltage at the highest thrust efficiency satisfying the criterion on impurity emission. In the cases violating this criterion, anode fall voltages are high, as observed in Fig. 5. The electrode phenomena are explained in the light of vacuum arc results.[6,7] When the discharge current is small, the anode space charge is neutralized by the ions emanating from the cathode spot and the anode fall voltage is kept low. As the current is increased, the anode sheath is more and more starved for ions and the anode fall voltage is increased. The ions ejected from the cathode are repelled by the anode fall potential. If the current is further increased, the incoming ions are completely repelled toward the cathode and the anode spot appears as a source of atoms and ions. Once the anode spot is formed, the anode space charge is neutralized and discharge voltage drops drastically. This phenomenon was also observed in the present experiment, in Fig. 5. Voltage stall corresponding to the spot formation was observed more clearly in the anode fall results in the same figure. As mass flow rate decreased, the current corresponding to the beginning of the voltage stall diminished. It was also informative that the maximum voltage prior to the stall corresponded to the condition just exceeding the criterion on impurity spectral emission. It can be easily understood from the foregoing discussion that in the AII/CI = 0/10 case the anode region was extremely starved and the anode fall voltage was large even at low current.

When the propellant was injected near the anode surface, the anode space charge was neutralized by the ions of propellant, as shown in Fig. 6 for the AII/CI = 7/3 case. The anode fall voltage was efficiently suppressed in this case. In Fig. 6, only the anode fall result corresponding to $\dot{m} = 0.16$ g/s and $J = 9.0$ kA indicated a voltage as high as 65 V. In this condition, the intensity of the WI and CuI lines showed a rapid increase and became comparable to that of the ArII line. Even in this condition the cathode fall voltage stayed below 30 V. It is, therefore, hardly conceivable that the argon ion is accelerated in the cathode fall and yields a tungsten atom by sputtering. If the argon ion is assumed to be accelerated in the anode sheath, on the other hand, 60-100 eV is reasonable as the minimum energy required for the argon ion to yield a tungsten atom by sputtering.[8] Assuming this mechanism to be effective, it is questioned if the anode sheath has an influence on cathode phenomena. For a mass flow rate of 0.2 g/s, a cross-sectional area of 9 cm^2, and an average axial velocity of 30 km/s, the plasma density n in the discharge chamber is estimated to be 10^{14} cm^{-3}. From Spitzer's formula for ion-ion collision time[9]

$$\tau = 11.4 A^{1/2} T_i^{3/2} / n Z^4 \ell n \Lambda, \text{ s} \tag{4}$$

$\tau = 6.8 \times 10^{-5}$ s is obtained for 100 eV Ar$^+$, where A is atomic weight, T_i is temperature or energy in K, $\ell n \Lambda \simeq 10$, and Z is ionic charge in units of proton charge. $Z = 1$ is assumed. The argon ion of 100 eV energy moves at 22 km/s, and the mean free path is found to be 1.5 m. This figure, which is much larger than the dimension of the discharge chamber, does not directly mean argon ion bombardment on the cathode surface at 100 eV. The self-magnetic field deflects the radial ion motion to axial and serves as a buffer against bombardment. The ion Larmor radius is 2.3 cm at the strongest magnetic field and is comparable to the cathode-anode separation. Near the base of the discharge chamber the ions are strongly deflected, whereas near the cathode tip this effect is inefficient. The ions are also accelerated by the radial electric field outside the anode sheath. This acceleration may intensify the bombardment effect.

The foregoing discussion reminds the authors of collisionless thrust generation.[10] The case AII/CI = 0/10, where the discharge voltage and the thrust are larger than in the other cases, possibly involves a collisionless mechanism. In this case, the propellant injected from the cathode root is confined near the cathode surface by the pumping force and is prevented from diffusing into the interelectrode region. Collisionless acceleration has to be provided with the following features:

1) The ion mean free path is larger than the dimension of the discharge chamber.

2) The ion Larmor radius is comparable to the dimension of the discharge chamber.

3) Both discharge voltage and thrust are proportional to J^2.

4) The ion velocity U is given by

$$U \leq (2\text{eV}/m_i)^{1/2} \tag{5}$$

where m_i is ion mass.

5) The discharge current is carried by the ions.

The first and second conditions are satisfied, as discussed earlier. The third condition is also satisfied, as shown in Figs.

2 and 5, although this condition is also true in the other operating conditions. The fourth condition is satisfied as far as the criterion on impurity emission is valid. The fifth condition is strongly violated. The current that can be carried by the ion flow is less than 10% of the discharge current. Assuming the collisionless acceleration is effective, the last figure implies that thrust efficiency is less than 10%. The rest of the current is carried by electrons, and the associated power is wasted. It was concluded from the preceding discussion that collisionless acceleration may occur in the AII/CI = 0/10 case but is very inefficient in the present scheme.

To summarize the effect of propellant distribution in the discharge chamber, maximum thrust efficiency is plotted against fractional mass flow rate from the cathode region or anode region in Fig. 13. The open circles indicate the maximum efficiency satisfying the criterion on impurity spectral emission. The solid circles correspond to the condition just violating the criterion. Apparently, in the AII/CI = 0/10 case, efficiency is low because of anode starvation. As the propellant supply from the anode region is increased, efficiency is increased and saturates above 70% propellant flow rate of AII. Maximum efficiency occurs at AII/CI = 10/0. The open triangles plotted at AII/CI = 5/5 and AII/CI = 10/0 represent maximum efficiency at AIO/CI = 5/5 and AIO/AII = 5/5, respectively. It can be said from these results that AIO injection is not as effective as AII in controlling anode fall.

Conclusions

In this experiment on a new MPD arcjet, KOMABA III, the following results were obtained:

1) Propellant injection near the anode surface is efficient in reducing anode fall voltage and enhancing thrust efficiency.

2) Propellant injection near the cathode surface emphasizes the collisionless features, but thrust efficiency is low.

3) Maximum efficiency is obtained with all propellant supplied from the anode root.

4) Having the sleeve electrode at floating potential coaxially mounted to the cathode was found to be useful in buffering current concentration.

References

[1] Rudolph, L. K., Jahn, R. G., Clark, K. E., and von Jaskowsky, W. F., "Onset Phenomena in Self-Field MPD Arcjets," AIAA Paper 78-653, April 1978.

[2] Krülle, G. and Zeyfang, E., "Preliminary Conclusions of Continuous Applied Field Electromagnetic Thruster Research at DFVLR," AIAA Paper 75-417, March 1975.

[3] Kuriki, K. and Suzuki, H., "Quasisteady MPD Arcjet with Anode Gas Injection," AIAA Paper 79-2058, Oct.-Nov. 1979.

[4] Kuriki, K., Kunii, Y., and Shimizu, Y., "Current Distribution in Plasma Thruster," AIAA Paper 80-0685, April 1980.

[5] Kuriki, K. and Suzuki, H., "Transitional Behavior of MPD Arcjet Operation," AIAA Paper 76-1002, Nov. 1976; also *AIAA Journal*, Vol. 16, Oct. 1978, pp. 1062-1067.

[6] Miller, H. C., "Vacuum Arc Anode Phenomena," *IEEE Transactions in Plasma Science*, Vol. PS-5, Sept. 1977, pp. 181-196.

[7] Kimblin, C. W., "Anode Phenomena in Vacuum and Atmospheric Pressure Arcs," *IEEE Transactions in Plasma Science*, Vol. PS-2, Dec. 1977, pp. 310-319.

[8] Laegreid, N. and Wehner, G. K., "Sputtering Yields of Metals for Ar^+ and Ne^+ Ions with Energies from 50 to 600 eV," *Journal of Applied Physics*, Vol. 32, March 1961, pp. 365-369.

[9] Spitzer, L. Jr., *Physics of Fully Ionized Gases*, Interscience, New York, 1962, Chap. 5.

[10] Stratton, T. F., "High Current Steady-State Coaxial Plasma Accelerators," *AIAA Journal*, Vol. 3, Oct. 1965, pp. 1961-1963.